Crystal structure of the photosensing module from a red/far-red light-absorbing plant phytochrome

E. Sethe Burgie, Adam N. Bussell, Joseph M. Walker, Katarzyna Dubiel, and Richard D. Vierstra[1]

Department of Genetics, University of Wisconsin-Madison, Madison, WI 53706

Edited by Peter H. Quail, University of California, Berkeley, Albany, CA, and approved May 23, 2014 (received for review February 18, 2014)

Many aspects of plant photomorphogenesis are controlled by the phytochrome (Phy) family of bilin-containing photoreceptors that detect red and far-red light by photointerconversion between a dark-adapted Pr state and a photoactivated Pfr state. Whereas 3D models of prokaryotic Phys are available, models of their plant counterparts have remained elusive. Here, we present the crystal structure of the photosensing module (PSM) from a seed plant Phy in the Pr state using the PhyB isoform from *Arabidopsis thaliana*. The PhyB PSM crystallized as a head-to-head dimer with strong structural homology to its bacterial relatives, including a 5(*Z*)*syn*, 10(*Z*)*syn*, 15(*Z*)*anti* configuration of the phytochromobilin chromophore buried within the cGMP phosphodiesterase/adenylyl cyclase/FhlA (GAF) domain, and a well-ordered hairpin protruding from the Phy-specific domain toward the bilin pocket. However, its Per/Arnt/Sim (PAS) domain, knot region, and helical spine show distinct structural differences potentially important to signaling. Included is an elongated helical spine, an extended β-sheet connecting the GAF domain and hairpin stem, and unique interactions between the region upstream of the PAS domain knot and the bilin A and B pyrrole rings. Comparisons of this structure with those from bacterial Phys combined with mutagenic studies support a toggle model for photoconversion that engages multiple features within the PSM to stabilize the Pr and Pfr end states after rotation of the D pyrrole ring. Taken together, this *Arabidopsis* PhyB structure should enable molecular insights into plant Phy signaling and provide an essential scaffold to redesign their activities for agricultural benefit and as optogenetic reagents.

Given the importance of sunlight to their survival and growth, plants have adopted a collection of photoreceptors and interconnected signaling cascades to optimize their photosynthetic potential and synchronize their lifecycles with circadian and seasonal rhythms. Chief among these are the phytochromes (Phys), a family of bilin (or open-chain tetrapyrrole)-containing red/far-red light-absorbing photoreceptors that provides spatial and time-dependent information by sensing the fluence rate, direction, duration, and color of a plant's light environment (1, 2). This information then regulates nearly all aspects of plant growth and development from seed germination to senescence. Notably, seed plants typically express three Phy isoforms (PhyA, PhyB, and PhyC) that control distinct and overlapping photoresponses, with PhyB having a dominant role in green tissues (2, 3).

Phys are homodimers with each sister polypeptide divided into an N-terminal photosensory module (PSM) that absorbs light followed by an output module (OPM) that promotes dimerization and presumably, relays the light signals (1, 4). The PSM sequentially contains a Per/Arnt/Sim (PAS) domain of unknown function, a cGMP phosphodiesterase/adenylyl cyclase/FhlA (GAF) domain that cradles the bilin, and a Phy-specific (PHY) domain that stabilizes the photoactivated state (Fig. S1). The OPM in plant Phys harbors consecutive PAS, PAS, and histidine kinase-related domains that might participate in signaling through interactions with downstream effectors and/or by a currently enigmatic kinase activity (1, 4).

Plant Phys use phytochromobilin (PΦB) as the chromophore, which is bound by a thioether linkage to a conserved GAF domain cysteine using an intrinsic lyase activity. It is synthesized in a biologically inactive, red light-absorbing Pr state, which converts on photoexcitation to a far-red light-absorbing Pfr state that is biologically active. A proposed key step involves a light-driven *Z* to *E* isomerization of the C15 = C16 bond in PΦB that rotates the D pyrrole ring, which presumably initiates conformation changes within the bilin-binding pocket that reverberate to the OPM (1, 4). Pfr rapidly converts back to Pr with far-red light or slowly by spontaneous thermal reversion, thus allowing Phys to act as both short- and long-lived photoswitches. Pr→Pfr photoconversion also triggers movement of Pfr from the cytosol to the nucleus, where it extensively reprograms plant gene expression mainly by promoting turnover of a family of Phy-Interacting Factor (PIF) transcriptional repressors (2).

Whereas atomic-level information is sparse for plant Phys beyond analyses on the chromophore moiety (5, 6), crystal and solution 3D structures of PSM fragments from proteobacterial (BphP) and cyanobacterial (Cph) relatives (7–16) and a single-particle EM image of an entire BphP (17) have provided useful surrogates. These models confirmed the predicted PAS and GAF folds and identified an intricate network of hydrogen bond and van der Waals interactions between the GAF domain pocket, the bilin, and several ordered waters (4). They also revealed an unusual figure-of-eight knot at the PAS/GAF domain interface, a distinctive hairpin (or tongue) that extends from the PHY domain to the bilin-binding pocket, and a helical spine that provides an elongated dimerization interface, all of which might underpin signal transmission. The chromophore in canonical BphPs/Cphs assumes a 5(*Z*)*syn*, 10(*Z*)*syn*, 15(*Z*)*anti* configuration as Pr, with the D ring substantially out of plane. Although the details of bacterial Phy photoconversion are complicated by structural variation, light-driven rotation of one or more pyrrole rings induces sliding of the bilin within the GAF

Significance

Much of plant growth and development is regulated by the phytochrome (Phy) family of photoreceptors. We present an atomic perspective of plant Phy signaling through a crystal structure of the photosensing module as Pr from *Arabidopsis* PhyB assembled with its native chromophore phytochromobilin. Although its overall architecture and chromophore/protein contacts are reminiscent of bacterial relatives, significant structural differences are seen within the prominent knot, hairpin and helical spine features. Subsequent mutational analyses lend support to a toggle model for how Phys reversibly switch between their Pr and Pfr end states. This 3D structure along with the identified suite of photochemical variants should accelerate the rational redesign of Phy signaling for improved crop performance and optogenetic application.

Author contributions: E.S.B., A.N.B., J.M.W., and R.D.V. designed research; E.S.B., A.N.B., J.M.W., and K.D. performed research; E.S.B., A.N.B., J.M.W., K.D., and R.D.V. analyzed data; and E.S.B. and R.D.V. wrote the paper.

The authors declare no conflict of interest.

This article is a PNAS Direct Submission.

Data deposition: The crystallography, atomic coordinates, and structure factors have been deposited in the Protein Data Bank, www.pdb.org (PDB ID code 4OUR).

[1]To whom correspondence should be addressed. Email: vierstra@wisc.edu.

This article contains supporting information online at www.pnas.org/lookup/suppl/doi:10.1073/pnas.1403096111/-/DCSupplemental.

BIOCHEMISTRY

domain, which likely impinges on the hairpin and helical spine features (7, 10, 13, 15, 18, 19). Bacterial Phy OPMs typically end in prototypic signaling motifs, such as two-component histidine kinase, diguanyl cyclase, and two-helix output sensor domains, to implicate the participation of Pfr (or Pr) in established signaling cascades (4, 14, 20).

Presently, it remains unclear how well these bacterial structures mimic plant Phys given significant differences in sequence and domain architecture. Examples include a long N-terminal extension (NTE) in plant Phys and pervasive sequence variations within the PAS, GAF, and PHY domains and the downstream OPM (3, 4). For a more authoritative view, we present the crystal structure of a Phy PSM from a seed plant, that of PhyB from *Arabidopsis thaliana*, and extensively characterize its solution and photochemical properties. Although the PSM behaves as a monomer in solution, it crystallized as a head-to-head dimer through a helical interface involving sister GAF domains. PhyB shares many features common to its bacterial relatives (4), thus implying similar photochemistry, but harbors several novel aspects, including an unanticipated interaction between the bilin and the NTE and a distinctive transition between the PAS and GAF domains that extends the helical spine. Site-specific mutants highlight the importance of many of these features and support a toggle model for photoconversion, where light-induced rotation of the D pyrrole ring ultimately impacts the OPM through considerable reconfiguration of the hairpin. Collectively, these data provide a coherent template to better understand and manipulate plant Phy signaling.

Results and Discussion

Overall Structure of the *Arabidopsis* PhyB PSM. Among the seed plant Phy isoforms, PhyB (and its PhyD paralog in *A. thaliana*) is distinguished by a long glycine/serine-rich NTE (3). We expressed the *Arabidopsis* PhyB PSM minus much of this possibly flexible region using a recombinant system that simultaneously synthesizes PΦB (21). PhyB(90–624) efficiently bound PΦB covalently, was stable in solution, displayed Pr and Pfr absorption spectra expected of a plant PhyB (21, 22), and retained Pr→Pfr and Pfr→Pr photoconversion kinetics similar to the full-length PSM (residues 1–624) (Fig. S1). However, it showed a 7-nm hypsochromic shift in Pfr absorption and strongly accelerated Pfr→Pr thermal reversion, supporting the import of the NTE to Pfr stability (1, 4). Absorption spectra of Pr and Pfr for the full PSM after acidic denaturation were consistent with the 15*Z* and 15*E* isomers of PΦB, respectively (Fig. S2).

PhyB(90–624) crystals enabled collection of a complete X-ray dataset to 3.4-Å resolution. Molecular replacement using the PAS/GAF region from *Synechocystis* (*Syn*) -Cph1 (9) allowed solution of initial phases. After molecular replacement, the calculated electron density was of sufficient quality to construct the remainder of the structure. Fig. S4 *C–E* shows representative electron density maps, and Table S1 shows statistical support.

Whereas PhyB(90–624) crystallized as a head-to-head dimer, both equilibrium sedimentation and size-exclusion chromatography (SEC) of the full PSM fragment revealed a monomeric size in solution as both Pr and Pfr (Fig. 1*A* and Fig. S3). SEC supported an elongated shape for the crystallographic subunits by estimating a Stokes radius ∼1.3 times that predicted. Analogous to several BphPs (12, 13, 17), the dimerization interface involved the GAF domain α1/α2/α6-helical bundle (Fig. 1*A* and Fig. S4*A*), suggesting that these contacts are pertinent to PhyB homodimerization but insufficient without the OPM. The sister PHY domains also contributed to the dimer interface through helix-α1 of subunit B and helix-α6 of subunit A.

The *Arabidopsis* PhyB PSM structure (Protein Data Bank ID code 4OUR) shares its core PAS-GAF-PHY domain architecture with canonical BphPs/Cphs (9, 11–13) with the inclusion of unique features in each domain (Fig. 1*A*). β-Sheet components of the PAS and GAF domains superposed reasonably well with those from *Syn*-Cph1, *Deinococcus radiodurans* (*Dr*) -BphP, and *Pseudomonas aeruginosa* (*Pa*) -BphP (Fig. S4*B* and Table S2).

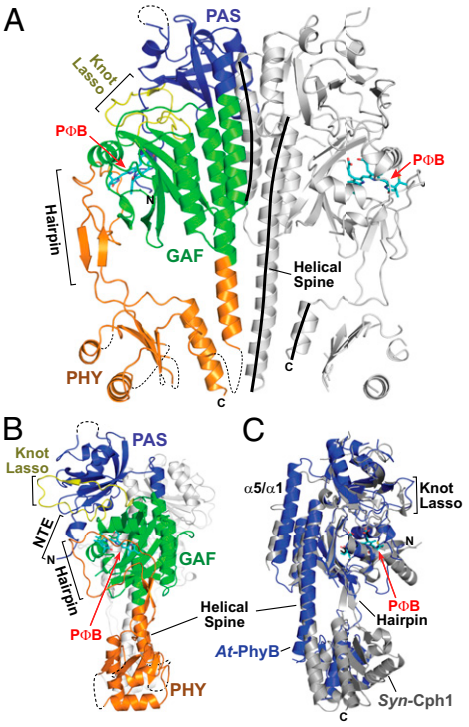

Fig. 1. Crystallographic structure of the PSM from *Arabidopsis* (*At*) PhyB as Pr and comparison with that from *Synechocystis* (*Syn*)-Cph1. (*A and B*) Ribbon diagram of the PSM dimer (residues 90–624) in (*A*) front and (*B*) side views. The PAS, GAF, and PHY domains in subunit A are colored in blue, green, and orange, respectively. The knot lasso (yellow), hairpin, helical spine, and NTE are indicated. PΦB (cyan) with its linkage to C357 is shown in stick form with the oxygens colored in red. The proposed connectivities of polypeptide regions not resolved in the crystal structure are indicated by the dashed lines for subunit A. (*C*) Superposition of PSMs from PhyB (blue; Protein Data Bank ID code 4OUR) and *Syn*-Cph1 (gray; Protein Data Bank ID code 2VEA) (9). The extended α5/α1-helix separating the PAS and GAF domains in PhyB is shown.

The PAS domains of sister PhyB subunits were highly congruent throughout, but in superpositions with bacterial Phys, the helical region between strands-β2 and -β3 varied substantially. PhyB also includes a large flexible loop comprising residues 145–155 (150s loop) after PAS helix-α1 (Fig. S4*A*). Prior phenotypic analysis of a P149-L mutant implied that this loop is significant to PhyB signaling but innocuous to its photochemistry (23). In addition, the neighboring M159 side chain contributes distinctive hydrophobic interactions with residues 335–337 of the GAF domain knot lasso. This interaction might stabilize the knot motif of PhyB, which has been implicated in PIF binding (24).

The PhyB GAF domain aligned well with those from bacterial Phys (Table S2). Significant differences in PhyB included an extended loop that encompasses residues 379–393 (380s loop) (Fig. S4*A*) and a distinctive lasso, with a shape that generated a more extensive antiparallel β-strand interaction with PAS strand-β2. The α-helix connecting the PAS and GAF domains (PAS helix-α5/GAF helix-α1) is longer than the analogous helix in bacterial Phys by three rotations. This addition substantially extends the helical spine to cover the full length of the PSM (Fig. 1*B*).

Electron density for the PHY domain was less resolved, especially in the loop regions (Fig. 1 and Fig. S4*E*); we presume that scarcity of crystal contacts in this region compromised resolution by enabling domain wobble within the crystal lattice. A lack of connectivity and side-chain features necessitated naming PHY domain residues in helix-α3 and helix-α5 as unknown for subunit B. By contrast, the signature PHY domain hairpin was

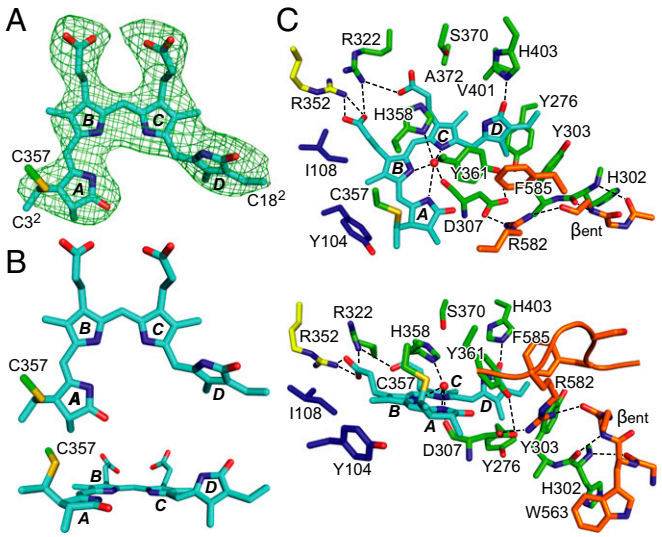

Fig. 2. Conformation of PΦB and its surrounding amino acids within the bilin-binding pocket of *Arabidopsis* PhyB. (*A*) Top view of PΦB superimposed on an Fo-Fc omit map of the chromophore region contoured at 3 σ. Blue, nitrogens; cyan, carbons; red, oxygens; yellow, sulfurs. (*B*) Top and side views of PΦB in a 5(*Z*)*syn*, 10(*Z*)*syn*, 15(*Z*)*anti* configuration and linked by a thioether bond between the $C3^1$ carbon and C357. Pyrrole rings A–D, the $C3^2$ methyl, and the $C18^2$ carbon of the D-ring vinyl are labeled. (*C*) Top and side views of the bilin-binding pocket of PhyB highlighting the positions of key amino acids. Residues from the PAS knot, PAS and NTE, GAF, and hairpin regions are colored yellow, blue, green, and orange, respectively. Dashed lines indicate hydrogen bonds.

well-defined and consistent between sister subunits, with a central feature being a stem formed by two antiparallel β-strands designated β_{ent} and β_{exit} (Fig. S4 *A* and *C*). The sister subunits of PhyB(90–624) had different overall shapes that yielded a superposed rmsd of 1.6 Å over all matching α-carbons. Because the individual domains were highly congruent, this difference manifested itself at the domain transitions, especially at the junction between GAF and PHY domains.

PΦB and the Bilin-Binding Pocket. The bilin and its GAF-domain pocket in PhyB shared strong homology with previously characterized bacterial Phys in the Pr state (7–12). As expected (1), PΦB was attached by a thioether bond to C357 through its $C3^1$ atom (Fig. 2 *A* and *B*). The electron density placed PΦB in the 5(*Z*)*syn*, 10(*Z*)*syn*, 15(*Z*)*anti* configuration in agreement with prior homology modeling and NMR analyses of plant PhyA (5, 6). The A–C pyrrole rings were mostly coplanar, and the D ring was rotated out of this plane by 58° (Fig. 2*A*). Dihedral angles about the C15 = C16 bond averaged 35° at this low resolution vs. 42° calculated from resonance Raman spectroscopy of *Arabidopsis* PhyA (5). A web of hydrogen bond and van der Waals interactions involving a constellation of conserved amino acids (e.g., Y104, I108, Y276, Y303, D307, R322, R352, H358, Y361, and H403 in PhyB) and the central pyrrole water grasped the bilin in the GAF pocket (Fig. 2*C*).

Mutational analyses with *Arabidopsis* PhyB by us and others (21–23) confirmed the importance of several key residues around PΦB. Although various point mutations altered the end states of photoconversion, most mutants had little impact on initial photochemistry, implying that the first reaction step(s) are relatively insensitive to the protein environment. In contrast, a number of mutations greatly influenced Pfr→Pr thermal reversion (Figs. 3 and 4, Figs. S5 and S6, and Table S3). Substitutions of D307 within the invariant Asp-Ile-Pro (DIP) motif and H358, which are focal points of the A–C pyrrole ring hydrogen-bond network and likely involved in the protonation/deprotonation cycle of the bilin (25), assembled hypsochromic-shifted Pr states (Fig. 3*B* and Fig. S6*B*). The D307-A mutation precluded photoconversion to Pfr and instead, led to a bleached species, and the H358-A biliprotein was partially photochromic but expressed poorly to suggest folding challenges. The D pyrrole ring is surrounded by H403 and a collection of bulky aromatic residues (Y276, Y303, and Y361) (Fig. 2*C*). The ε-nitrogen of H403 makes a crucial hydrogen bond with the carbonyl of the D ring, thus anchoring the D ring in its Pr-state position. The Y276-H substitution created a photochemically inert fluorescent variant as reported (22), whereas the H403-A and Y361-F substitutions had strong opposite effects on Pfr thermal reversion (Figs. 3*B* and 4) (21).

As in bacterial Phys, the B-ring carboxylate bound a nearby arginine (R352). Accordingly, the R352-A substitution generated small hypsochromic shifts in Pr and Pfr absorption with unaltered Pr/Pfr photointerconversion rates, but Pfr was markedly

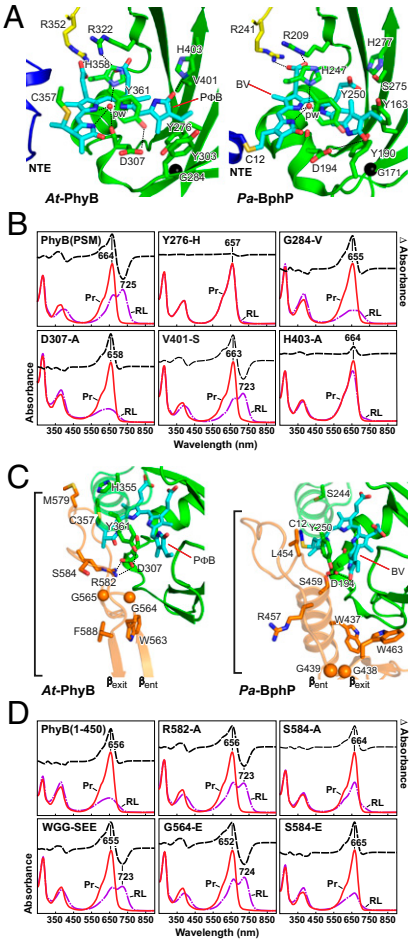

Fig. 3. Structural and mutational analysis of key amino acids surrounding the bilin and the PHY domain hairpin in *Arabidopsis* (*At*) PhyB. (*A* and *C*) Close-up views of the (*A*) GAF domain and (*C*) hairpin in PhyB and *Pseudomonas aeruginosa* (*Pa*)-BphP as Pfr (Protein Data Bank ID code 3C2W) (16). The bilin, NTE, GAF, knot lasso, and PHY domain features and associated residues are colored in cyan, blue, green, yellow, and orange, respectively. The comparable amino acids between *At*-PhyB and *Pa*-BphP are labeled. Nitrogens and oxygens are colored in blue and red, respectively. Dashed lines indicate hydrogen bonds. Hairpin is indicated by bracket. The β_{ent}- and β_{exit}-strands connecting the hairpin to the rest of the PHY domain are labeled. BV, biliverdin; pw, pyrrole water. (*B* and *D*) UV-visible spectroscopy of selected PhyB(PSM) mutants affecting (*B*) the GAF domain and (*D*) the hairpin. Absorption and difference spectra were measured as Pr and after saturating red light irradiation (RL). Absorption maxima are indicated. Photoconversion and thermal reversion kinetics are shown in Fig. 4, Fig. S5, and Table S3.

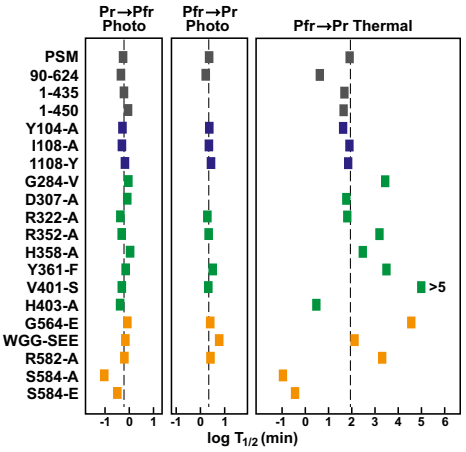

Fig. 4. Half-lives (*t*/2) for the Pr→Pfr and Pfr→Pr photoconversion reactions and Pfr→Pr thermal reversion for *Arabidopsis* PhyB PSM mutants and truncations. Rates were measured at 25 °C using the absorbance at 660 or 730 nm. Standardized red (660 nm) or far-red light (730 nm) fluence rates were used for photoconversion. With the exception of H385A, each square represents the average of three separate measurements. Dashed lines indicate the *t*/2 of unmodified PhyB(PSM). Mutants without data points represent those that failed to generate normal Pfr spectra upon photoconversion with red light. Blue boxes, NTE and PAS mutants; gray boxes, the full-length PhyB PSM or truncations; green boxes, GAF mutants; orange boxes, PHY hairpin mutants. Y276H was omitted because of impaired photochemistry.

slower at thermal reversion (Fig. S6 and Table S3) (21, 25). The C-ring propionate was parallel with the B-ring propionate and contacted the adjacent R322 (Fig. 2*C*) (5). This tether differs from bacterial Phys, where the C-ring propionate points away from the B-ring propionate (7, 9) to associate with a conserved histidine (H358 in PhyB), a pair of positionally conserved serine residues (positions 370 and 372 in PhyB), and an ordered water (Fig. 3*A*). Whereas *Arabidopsis* PhyB retained one of these serines (Ser370), the lack of a hydroxyl at position 372 might promote the B-ring propionate/R322 association. R322 is mechanistically relevant, because the alanine substitution displayed a 5-nm hypsochromic shift in Pfr absorption and an increased thermal reversion rate (Fig. 4, Fig. S6*B*, and Table S3) (21).

Stabilization of Pfr by the PHY Domain Hairpin. Consistent with studies of bacterial relatives (4, 25), the PHY domain in *Arabidopsis* PhyB is crucial for photochemistry, because a PΦB-bound PSM fragment missing the entire PHY sequence [PhyB(1–450)] generated normal Pr but failed to photoconvert to Pfr (Fig. 3*D*). As with several bacterial Phy structures (7, 9, 13, 14), the hairpin protrudes from the PHY domain toward the GAF domain as an extended loop between strand-β5 and helix-α6 (Figs. 1*A* and 3*C* and Fig. S4*A*). Strikingly, the hairpin intimately connects the PHY domain to the bilin-binding cleft by extending the GAF domain β-sheet by the two β-strands (β_{ent} and β_{exit}) contributed from the hairpin stem, and by providing intimate contacts at the core of the bilin/GAF domain interface through a salt bridge between R582 and D307 and a hydrophobic interaction between F585 and GAF helix-α5 (Fig. 3*C*). The 3D structure of the PhyB hairpin differs from the Pr-state bacterial Phys, because the loop-connecting strands β_{ent} and β_{exit} associate closely with the PhyB GAF domain throughout. As noted for *Syn*-Cph2 (7), the conserved WGG motif at the end of strand-β_{ent} further reinforces the stem structure by creating a tightly curved motif that presses its tryptophan (W563) against a GAF domain pocket formed by H283, H302, and the main chain of Y303.

Our mutational analyses of *Arabidopsis* PhyB revealed that the hairpin contacts are not essential to Pr but some residues are critical for proper Pr/Pfr interconversion and/or the thermal stability of Pfr (Figs. 3*D* and 4). Substitutions affecting the arginine and serine residues within the PRXSF sequence profoundly affected thermal reversion, with the R582-A mutant slowing thermal reversion by 25-fold and the S584-A and S584-E mutants strikingly increasing it by up to 750-fold. As proposed (7), the WGG motif also participates in Pfr stability. The G564E substitution, which should weaken or preclude the WGG motif/GAF domain interaction in Pr, slowed thermal reversion by ~450-fold (Fig. 4). A modest affect on thermal reversion was also seen by a wholesale change of WGG to SEE, which should disrupt the sharp turn provided by the WGG sequence and increase solvent exposure, but this substitution likely has pleiotropic consequences given that it was one of the few mutations that appreciably affected both Pr→Pfr and Pfr→Pr photoconversion (Fig. S5). The hairpin loop is also likely important based on prior analysis of the M579-T variant that greatly attenuates signaling *in planta* (26). Our 3D structure suggests that this threonine replacement stabilizes hairpin/GAF domain binding by an adventitious interaction with H355 (Fig. 3*C*).

Role of the PhyB NTE. Unlike most bacterial Phys, plant Phys contain a long glycine/serine-rich NTE that is critical to the normal absorption of the photoreceptor and stability of Pfr (1, 4) as well as biological activity, possibly through its light-dependent phosphorylation (27, 28). For example, NTE deletion mutants, such as PhyB(90–624), display hypsochromically shifted absorption maxima and more rapid thermal reversion (Fig. S1 *D* and *F*). Some of these effects might be explained by our 3D model of PhyB(90–624), which revealed that part of the NTE contacts the GAF domain near the bilin crevice (Fig. 1*A*). In particular, an α-helix encompassing residues 104–110 forms a steric barrier for the A and B pyrrole rings with conserved residues Y104 and I108 directly abutting the bilin (Fig. 2*C*). Accordingly, the Y104-A, I108-Y, and I108-A substitutions yielded PSMs with hypsochromically shifted Pr and Pfr absorption spectra (~3–8 nm), with the Y104-A mutant also accelerating thermal reversion by twofold (Fig. 4, Fig. S6, and Table S3). Y104 was previously shown to be key to PhyB nuclear localization and photoactivity *in planta* through its Pfr-dependent phosphorylation (27). Y104 is buried in our Pr structure, suggesting that light-induced reorganization of the NTE/hairpin underpins its modification.

Comprehensive Toggle Model for PhyB Photoconversion. A defining feature of Phys among biological photoreceptors is their ability

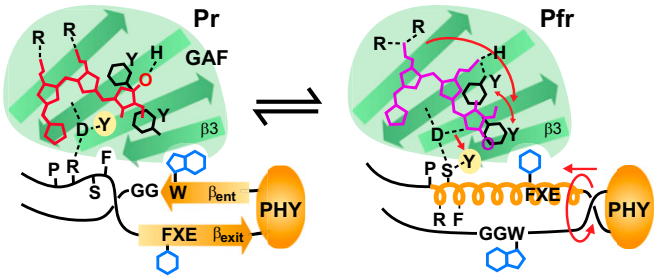

Fig. 5. Toggle model for Phy photoconversion that translates light into a conformational signal. After light-induced rotation of the D pyrrole ring, the bilin breaks its D-ring/H403 connection and slides within the GAF domain crevice to form a new contacts between the D ring and D307 and between the C-ring propionate and H403. Y276 and Y303, adjacent to the D ring, rotate in directions opposite to the D-ring rotation. Together, the effects initiate a collision of Y361 with F585, breakage of the D307/R582 contact, and other changes that collectively release the hairpin stem from the GAF domain. The hairpin stem then becomes helical, swivels, reforms a new contact between D307 and S584 in the PRXSF motif, and swaps the β_{ent} for a β_{exit} F588 connection with the GAF domain surface. The rotation and helical conversion of strand-β_{exit} presumably reorient the PHY domain relative to the GAF domain and/or tug on the helical spine connecting the PHY domain to OPM to eventually actuate signaling by the OPM. FXE, Phe-X-Glu; WGG, Trp-Gly-Gly. Modified from refs. 6–8, 13, 15, and 29.

to reversibly photoconvert between two relatively stable end states. By comparing the PSM structures from two Phys that use Pr as the dark-adapted state (7, 9) and two bathyphytochromes that assume a Pfr-like state without photoexcitation (*Pa*-BphP and *Rhodopseudomonas plaustris*-BphP1) (13, 14, 19), Anders et al. (7) recently proposed a "tryptophan switch" model for photoconversion (Fig. 5) (7). Here, light-induced rotation of the D pyrrole ring disrupts the connection between the GAF domain residue D307 and R582 in the hairpin PRXSF motif. The β_{exit}-strand capped by the PRXSF proline becomes helical and swivels to promote a new contact between the adjacent S584 residue in the hairpin and D307 and a positional swap of two tryptophans, in which W563 from the strand-β_{ent} WGG motif releases from the GAF domain surface and is replaced by a second bulky hydrophobic residue (F588 in a FXE motif in PhyB) within strand-β_{exit} of the stem. Conversion of the hairpin from β-stranded to helical then impacts the OPM by reversibly altering the GAF/PHY domain connections. This β-strand to helical refolding was recently confirmed by low-resolution paired Pr and Pfr crystal structures of the PSM from *Dr*-BphP, which in turn, supported a large-scale separation of the sister PHY domains within the dimer (29).

Our analyses of *Arabidopsis* PhyB support this model for Phys with PAS/GAF/PHY domain architectures and extend it to other PSM features that promote the Pr/Pfr transitions and stabilize the two end states (Fig. 5). Isomerization-driven rotation of the D pyrrole ring seems essential to photointerconversion of canonical Phys (18, 19). The D ring is chemically asymmetric with hydrophobic methyl and vinyl groups on one side of the methine bridge and hydrophilic nitrogen and carbonyl moieties on the other side. In Pr, the hydrophilic face binds the H403 imidazole through its carbonyl, and the pyrrole nitrogen likely interacts with solvent (7, 9, 12), whereas the hydrophobic face is surrounded by a compatible hydrophobic surface provided by M274, Y276, Y303, and M365 (Fig. 2*C*). A 180° rotation would then expose the D-ring functionalities to a nonideal environment, which recovers by sliding the bilin within the GAF pocket as illustrated in the paired end-state GAF domain models from the Phy relative PixJ from *Thermosynechococcus elongatus* and the PSM of *Pa*-BphP (8, 13, 15, 19).

Bilin sliding then induces a cascade of bilin/protein and protein/protein alterations that ultimately impinge on the hairpin (Fig. 5). From comparisons of Phy structures as Pr with that from *Pa*-BphP as Pfr, Yang et al. (13, 19) noted that the tyrosine pair (Y276 and Y303) abutting the D-ring methyl and vinyl groups counterrotate on D-ring flip. The photochemical necessity of these tyrosines and their rotations is vividly illustrated by the PhyB Y276-H and G284-V substitution. The Y276-H biliprotein is completely blocked in photoconversion but induces *Arabidopsis* photomorphogenesis without light, suggesting that it assumes a Pfr-like signaling state without photoexcitation (Fig. 3*B*) (22). The subtle G284-V substitution tested here generates a strongly stable but bleached species in red light, presumably by sterically hindering proper rotations of Y276 and Y303 (Figs. 3*B* and 4). Bilin sliding would also reorient the B- and C-ring propionates to attain positions similar to those found in the Pfr state of the bathyphytochromes *Pa*-BphP and *Rhodopseudomonas plaustris*-BphP1 (13, 14). Whereas the B-ring propionate would move subtly to generate a new contact with R322, the C-ring propionate would move dramatically to engage H403 after it breaks from the D-ring nitrogen. In *Pa*-BphP (13), an adjacent serine residue stabilizes its Pfr ground state, presumably by enforcing the position of *ZZEssa* configuration of the Pfr bilin through contact with the C-ring propionate (Fig. 3*A*). Remarkably, serine replacement of the complementary residue in *Arabidopsis* PhyB (V401) also generated a strongly stable Pfr state. Although this V401-S variant had relatively normal Pr and Pfr photochemistry, its thermal reversion was undetectable even after 2 d at 25 °C (Figs. 3*B* and 4 and Fig. S5*C*).

From the survey of Phy models (7–11, 13–15) (this study), it seems that both bilin sliding and D-ring photoisomerization impact the positions of D307 and Y361, in which D-ring rotation repositions the Y361 hydroxyl group away from the carboxyl moiety of D307 and D307 forms a hydrogen bond with the Pfr-state D-ring nitrogen. Although the subtle movement of D307 between superposed Pr and Pfr structures would suggest preservation of the D307/R582 contact, the repositioned Y361 would collide with the conserved PRXSF residue F585. Additionally, strand-β3 of the GAF domain would move with Y276/Y303 repositioning, potentially compromising the GAF-β3/hairpin-β_{ent} interaction. Together, these effects presumably melt the GAF/hairpin interaction, including the D307/R582 salt bridge, to permit helical refolding of the stem. As proposed (7, 29), this refolding also would swivel the main-chain positions of the melted strands-β_{ent} and -β_{exit} with respect to the GAF domain and swap the positions of R582 and S584 to now allow hydrogen bonding between S584 and D307 (Fig. 5). The stem/GAF domain contact could also be renewed by association of the exit sequence and its FXE motif with the GAF domain β-sheet (7).

The importance of these R582, S584, and the WGG motif contacts is illustrated by the mutational studies with *Syn*-Cph1, *Syn*-Cph2, and *Pa*-BphP (7, 9, 13) and our studies with *Arabidopsis* PhyB (Figs. 3*D* and 4) (21). For example, compromising the proposed Pfr contact in PhyB through the S584-A and S584-E substitutions generated a bleached species in red light with substantially accelerated thermal reversion ($t/2 \sim 7$ and 22 s, respectively, vs. 83 min for WT) (Table S3). Loss of the NTE also exacerbated thermal reversion, indicating a key role in Pfr stabilization (Fig. 4). Although not essential to *Arabidopsis* PhyB photochemistry, effects of the G564-E and WGG-SEE mutations support the proposed tryptophan switch (7) that encourages Pr/Pfr photointerconversion and the thermal stability of Pfr (Figs. 3*D* and 4 and Table S3). The importance of WGG to PhyB signaling is dramatically illustrated by observations that the G564-E mutation increases the red-light sensitivity of *Arabidopsis* seedlings by as much as 1,000-fold (30).

We imagine that the light-induced hairpin reconfiguration strains the GAF/PHY domain interface as the stem swivels and impinges on the PHY/OPM interface as the stem contracts from its β-strand to α-helical configuration through a direct connection between the helical spine and strand-β_{exit}. Consequently, even a small tug on the hairpin stem could have profound implications on OPM activity by toggling the end state positions of sister OPMs relative to the PSM and each other. For *Dr*-BphP, this strain substantially splays the sister PHY domains that likely amplify into nanometer-scale reorientations of the sister OPMs (29).

Conclusions

Our 3D structure for the PSM of *Arabidopsis* PhyB now offers a useful template to appreciate how plant Phys function mechanistically and the molecular effects underpinning the myriad of Phy signaling mutants (21–24, 26, 27, 30). Compared with the 3D models from bacterial relatives, a common architecture for Phy-type photoreceptors emerges along with the identification of plant Phy-specific features that might be critical for their interactions with downstream effectors (e.g., PIFs) (24, 27, 31). Collectively, these comparisons combined with mutagenic studies extend the tryptophan switch model for photoconversion (7) to include a dynamic interplay of additional features within the PSM in driving photoconversion and stabilizing the Pr and Pfr end states. Presumably, the resulting toggle between these end states encourages differential signaling output that informs plants about their light environment. With this PhyB PSM scaffold, the rational redesign of plant Phys for improved agricultural performance (21) and as optogenetic tools (31, 32) should accelerate.

Materials and Methods

Biliprotein Expression and Purification. *A. thaliana* PhyB PSM constructions bearing N- or C-terminal 6His tags and assembled with PΦB were expressed in *Escherichia coli* BL21-AI cells using a dual-plasmid expression system (21). For the

PSM constructions with N-terminal 6His tags, the MGSSHHHHHHSSENLYFQGH sequence bearing a tobacco etch virus (TEV) protease cleavage site was appended that resulted in a Gly-His extension after TEV protease cleavage. Cells were grown in the dark at 37 °C in terrific broth containing 0.4% glycerol and 1 mM $MgCl_2$, temperature was reduced to 16 °C, and then, the medium was made to 100 μM in δ-aminolevulinic acid. After 1 h, isopropyl β-D-1-thiogalactopyranoside was added to 1 mM followed by the addition of arabinose to 0.2% after a second hour to induce PΦB and apoprotein synthesis.

PhyB-expressing cells were sonicated and clarified, and the resulting extract was subjected to nickel-nitriloacetic acid chromatography (Qiagen) as described (8). PhyB constructions containing TEV-protease sites were cleaved overnight with recombinant TEV protease. The eluates were made to 200 mM in NH_2SO_4, applied to a butyl Sepharose HP column, and eluted with a linear 200- to 0-mM NH_2SO_4 gradient in 10% (vol/vol) glycerol, 10 mM 2-mercaptoethanol, and 20 mM Hepes (pH 7.8). PhyB fractions were exchanged into 10% (vol/vol) glycerol, 10 mM 2-mercaptoethanol, 20 mM NaCl, and 20 mM Hepes (pH 7.8) and purified with a Q-Sepharose HP column (GE) using a 20- to 500-mM linear NaCl gradient. Samples were exchanged into crystallization buffer containing 50 mM NaCl, 0.3 mM Tris(2-carboxyethyl)phosphine (TCEP), and 5 mM Hepes (pH 7.8) or standard assay buffer (SAB) containing 150 mM KCl, 0.3 mM TCEP, and 50 mM Hepes (pH 7.8 at 25 °C). Samples in SAB without TCEP were frozen and stored at −80 °C.

PhyB PSM Crystallography. PhyB(90–624) biliprotein bearing a C-terminal SLHHHHHH tag was crystallized by sitting drop vapor diffusion using the Hampton Index screen and PhyB in crystallization buffer. Well-ordered crystals were formed in solutions containing 15 mg/mL PhyB, 1.2 M $MgSO_4$, 4% (vol/vol) glycerol, 1% poly(ethylene glycol)3350, and 100 mM Bis·Tris (HCl) (pH 5.5). Crystals were exchanged into 100 mM $MgSO_4$, 25% PEG 3350, 15% PEG 550 monomethyl ether, and 100 mM Bis·Tris (pH 5.5) and flash cooled in liquid nitrogen. Final datasets were collected by the Life Sciences Collaborative Access Team at the Advanced Photon Source and indexed, integrated, and scaled using HKL2000 (33). Initial phases were calculated by PHASER (34) using the PAS-GAF region of *Syn*-Cph1 as the search model (Protein Data Bank ID code 2VEA) (9). Manual model building was conducted with COOT (35), refined with PHENIX (34) without real-space refinement and invoking noncrystallographic symmetry in torsion angle mode, and validated with MOLPROBITY (36). Superpositions were arranged with LSQKAB (37).

Equilibrium Sedimentation and SEC of PhyB(PSM). Equilibrium sedimentation was conducted at 20 °C in darkness with a Beckmann XL-A analytical ultracentrifuge and PhyB dissolved as Pr in SAB. SEC was conducted at 20 °C by FPLC (0.2 mL/min) with a 0.5 × 20-cm analytical grade Superdex 200 column (GE) equilibrated with SAB and 50 μL of either Pr samples or samples continuously irradiated with red light (mostly Pfr).

Spectroscopic Measurements. Absorption spectra and Pr/Pfr interconversion were measured at 25 °C in SAB (21). Red or far-red light was provided by 660- or 730-nm peak output light emitting diodes filtered through 10-nm half-peak width 660- or 730-nm interference filters, respectively. Absorption spectra after denaturation were recorded after dissolution in 8 M urea (pH 2.0).

ACKNOWLEDGMENTS. We thank Drs. Junrui Zhang and Andrew Ulijasz for advice on expression, Darrell McCauslin for help with equilibrium sedimentation, the University of Wisconsin Center for Eukaryotic Structural Genomics for access to its crystal screen facilities, and Drs. Craig Bingman and George Phillips for helpful discussions. This work was supported by National Science Foundation Grant MCB 1329956 and a grant from the University of Wisconsin College of Agricultural and Life Sciences (Hatch; to R.D.V.).

1. Rockwell NC, Su YS, Lagarias JC (2006) Phytochrome structure and signaling mechanisms. *Annu Rev Plant Biol* 57:837–858.
2. Franklin KA, Quail PH (2010) Phytochrome functions in Arabidopsis development. *J Exp Bot* 61(1):11–24.
3. Mathews S (2010) Evolutionary studies illuminate the structural-functional model of plant phytochromes. *Plant Cell* 22(1):4–16.
4. Vierstra RD, Zhang J (2011) Phytochrome signaling: Solving the Gordian knot with microbial relatives. *Trends Plant Sci* 16(8):417–426.
5. Mroginski MA, et al. (2011) Structure of the chromophore binding pocket in the Pr state of plant phytochrome phyA. *J Phys Chem B* 115(5):1220–1231.
6. Song C, Essen LO, Gärtner W, Hughes J, Matysik J (2012) Solid-state NMR spectroscopic study of chromophore-protein interactions in the Pr ground state of plant phytochrome A. *Mol Plant* 5(3):698–715.
7. Anders K, Daminelli-Widany G, Mroginski MA, von Stetten D, Essen LO (2013) Structure of the cyanobacterial phytochrome 2 photosensor implies a tryptophan switch for phytochrome signaling. *J Biol Chem* 288(50):35714–35725.
8. Burgie ES, Walker JM, Phillips GN, Jr., Vierstra RD (2013) A photo-labile thioether linkage to phycoviolobilin provides the foundation for the blue/green photocycles in DXCF-cyanobacteriochromes. *Structure* 21(1):88–97.
9. Essen LO, Mailliet J, Hughes J (2008) The structure of a complete phytochrome sensory module in the Pr ground state. *Proc Natl Acad Sci USA* 105(38):14709–14714.
10. Ulijasz AT, et al. (2010) Structural basis for the photoconversion of a phytochrome to the activated Pfr form. *Nature* 463(7278):250–254.
11. Wagner JR, Brunzelle JS, Forest KT, Vierstra RD (2005) A light-sensing knot revealed by the structure of the chromophore-binding domain of phytochrome. *Nature* 438(7066):325–331.
12. Wagner JR, Zhang J, Brunzelle JS, Vierstra RD, Forest KT (2007) High resolution structure of *Deinococcus* bacteriophytochrome yields new insights into phytochrome architecture and evolution. *J Biol Chem* 282(16):12298–12309.
13. Yang X, Kuk J, Moffat K (2009) Conformational differences between the Pfr and Pr states in Pseudomonas aeruginosa bacteriophytochrome. *Proc Natl Acad Sci USA* 106(37):15639–15644.
14. Bellini D, Papiz MZ (2012) Structure of a bacteriophytochrome and light-stimulated protomer swapping with a gene repressor. *Structure* 20(8):1436–1446.
15. Cornilescu CC, et al. (2014) Dynamic structural changes underpin photoconversion of a blue/green cyanobacteriochrome between its dark and photoactivated states. *J Biol Chem* 289(5):3055–3065.
16. Yang X, Kuk J, Moffat K (2008) Crystal structure of *Pseudomonas aeruginosa* bacteriophytochrome: Photoconversion and signal transduction. *Proc Natl Acad Sci USA* 105(38):14715–14720.
17. Li H, Zhang J, Vierstra RD, Li H (2010) Quaternary organization of a phytochrome dimer as revealed by cryoelectron microscopy. *Proc Natl Acad Sci USA* 107(24):10872–10877.
18. Song C, et al. (2011) Two ground state isoforms and a chromophore D-ring photoflip triggering extensive intramolecular changes in a canonical phytochrome. *Proc Natl Acad Sci USA* 108(10):3842–3847.
19. Yang X, Ren Z, Kuk J, Moffat K (2011) Temperature-scan cryocrystallography reveals reaction intermediates in bacteriophytochrome. *Nature* 479(7373):428–432.
20. Auldridge ME, Forest KT (2011) Bacterial phytochromes: More than meets the light. *Crit Rev Biochem Mol Biol* 46(1):67–88.
21. Zhang J, Stankey RJ, Vierstra RD (2013) Structure-guided engineering of plant phytochrome B with altered photochemistry and light signaling. *Plant Physiol* 161(3):1445–1457.
22. Su YS, Lagarias JC (2007) Light-independent phytochrome signaling mediated by dominant GAF domain tyrosine mutants of *Arabidopsis* phytochromes in transgenic plants. *Plant Cell* 19(7):2124–2139.
23. Oka Y, Matsushita T, Mochizuki N, Quail PH, Nagatani A (2008) Mutant screen distinguishes between residues necessary for light-signal perception and signal transfer by phytochrome B. *PLoS Genet* 4(8):e1000158.
24. Kikis EA, Oka Y, Hudson ME, Nagatani A, Quail PH (2009) Residues clustered in the light-sensing knot of phytochrome B are necessary for conformer-specific binding to signaling partner PIF3. *PLoS Genet* 5(1):e1000352.
25. Wagner JR, et al. (2008) Mutational analysis of *Deinococcus radiodurans* bacteriophytochrome reveals key amino acids necessary for the photochromicity and proton exchange cycle of phytochromes. *J Biol Chem* 283(18):12212–12226.
26. Maloof JN, et al. (2001) Natural variation in light sensitivity of *Arabidopsis*. *Nat Genet* 29(4):441–446.
27. Nito K, Wong CC, Yates JR, 3rd, Chory J (2013) Tyrosine phosphorylation regulates the activity of phytochrome photoreceptors. *Cell Reports* 3(6):1970–1979.
28. Medzihradszky M, et al. (2013) Phosphorylation of phytochrome B inhibits light-induced signaling via accelerated dark reversion in *Arabidopsis*. *Plant Cell* 25(2):535–544.
29. Takala H, et al. (2014) Signal amplification and transduction in phytochrome photosensors. *Nature* 509(7499):245–248.
30. Ádám É, et al. (2011) Altered dark- and photoconversion of phytochrome B mediate extreme light sensitivity and loss of photoreversibility of the *phyB-401* mutant. *PLoS ONE* 6(11):e27250.
31. Shimizu-Sato S, Huq E, Tepperman JM, Quail PH (2002) A light-switchable gene promoter system. *Nat Biotechnol* 20(10):1041–1044.
32. Levskaya A, Weiner OD, Lim WA, Voigt CA (2009) Spatiotemporal control of cell signalling using a light-switchable protein interaction. *Nature* 461(7266):997–1001.
33. Otwinowski Z, Minor W (1997) Processing of X-ray diffraction data collected in oscillation mode. *Methods Enzymol* 276:307–326.
34. McCoy AJ, et al. (2007) Phaser crystallographic software. *J Appl Cryst* 40(Pt 4):658–674.
35. Emsley P, Cowtan K (2004) Coot: Model-building tools for molecular graphics. *Acta Crystallogr D Biol Crystallogr* 60(Pt 12 Pt 1):2126–2132.
36. Chen VB, et al. (2010) MolProbity: All-atom structure validation for macromolecular crystallography. *Acta Crystallogr D Biol Crystallogr* 66(Pt 1):12–21.
37. Kabsch W (1976) A solution for the best rotation to relate two sets of vectors. *Acta Crystallogr A* 32(5):922–923.